Supporting Information for "Ni-Fe-S cubanes on CO_2 reduction electrocatalysis: A DFT study"

J. B. Varley[1,2], H. A. Hansen[1], N. L. Ammitzbøll[3], L. C. Grabow[1,4] A. A. Peterson[1,5] J. Rossmeisl[3] J. K. Nørskov[1,6]

[1]*Department of Chemical Engineering, Stanford University, Stanford, CA 94305-5025*

[2]*Lawrence Livermore National Laboratory, Livermore, California, 94550, USA*

[3]*Center for Atomic-scale Materials Design, Department of Physics, Technical University of Denmark, DK-2800 Lyngby, Denmark*

[4]*Department of Chemical and Biomolecular Engineering, University of Houston, Houston, TX 77204*

[5]*Department of Chemical Engineering, Brown University, Providence, RI 02912*

[6]*SUNCAT Center for Interface Science and Catalysis, Photon Science, SLAC National Accelerator Laboratory, Menlo Park, CA 94025*

September 4, 2013

1 Computational Methods

All reported calculations are based on density functional theory (DFT) using a real-space grid and projector-augmented wave (PAW) potentials as implemented in the GPAW code. [1, 2] The uniform grid-spacing was set to 0.18 Å for all calculations. Electron exchange and correlation terms were described with the use of the revised Perdew-Burke-Ernzerhof (RPBE) exchange-correlation functional. [3] All integrations over the Brillouin zone are performed using only the Γ-point for the $20 \times 20 \times 20$ Å non-periodic supercells. Geometries were optimized using the GPAW code and the ASE simulation environment and only the lowest energy adsorbate binding sites are reported. [4] All results were obtained with spin-polarized (spin-unrestricted) calculations. The electronic structure calculations employed a Fermi-level smearing width, taken as 0.05 eV for the adsorbates, and 0.01 eV for all gas-phase calculations. Tests using larger non-periodic $30 \times 30 \times 30$ Å supercells confirm that all reported binding energies are converged for the charged and uncharged clusters.

The cubane structures were optimized by relaxing different initial guesses of the structure without adsorbates. For the cubanes containing between 1 and 3 Ni, we found the different geometric arrangements of the possible Ni-Fe orderings to have a minor affect on the calculated energies with and without adsorbates. The intermediate structures were determined by relaxing the configurations of the cubane with the adsorbate placed at all the possible binding sites. In general, we find that COOH* most favorably adsorbs to S, OCHO* most favorably binds to Fe over Ni, and CO* most favorably binds to Ni over Fe. The obtained electronic energies were

Table S1: RPBE contributions to the adsorbate free energy from the zero-point energy correction, enthalpic temperature correction, entropy, and the total free energy correction, respectively. All values are given in eV.

Adsorbate	ZPE (eV)	$\int C_P\, dT$ (eV)	$-TS$ (eV)	$G - E_{\text{elec}}$ (eV)
COOH*	0.62	0.10	−0.19	0.53
OCHO*	0.63	0.10	−0.17	0.56
CO*	0.19	0.08	−0.16	0.11
H*	0.18	0.01	−0.01	0.18

converted to free energies on the basis of the calculated vibrational frequencies and standard statistical thermodynamics as described in Sections 1.1 and 1.2.

We note that the free energies are dependent on both the spin state and the charge state of the reaction structures and the results presented in Figures 2−5 of the main text are constructed using the lowest-energy spin states for a charge state of -2. To address the energy dependence on the local spin configuration, we varied both the magnetic and electronic spin contributions of the cluster to determine the lowest energy structure for a given charge state (see Section 1.3). For each geometrically distinct calculation, we tested all 2^4 permutations of up/down spin states on the four metal atoms in the cluster and report the corresponding lowest-energy electronic spin states. We do not place particular emphasis on the exact spin state of each intermediate structure, as we found several distinct spin configurations to be nearly degenerate in energy.

As the experimentally synthesized [Fe_4S_4] cubane structures are found to have a charge of -2, [5] we considered an extra charge of up to -2 for each cluster composition. Because the charge state of the clusters are strongly dependent on the chemical environment, such as the choice of support and electrolyte, we do not attempt to justify which charge states may be the most prevalent for a given cluster composition. We find that the addition of charge does have an effect on the calculated binding energies, where all of the studied cubanes favor the COOH* intermediate for the 0 and -1 charge states (see Section 1.3). In the context of the activity model of Ref. 6, the trends of the different cubane compositions all reflect the same qualitative conclusions, independent of the cluster charge state. Namely, the Ni-containing cubanes are predicted to be comparable to or more active than the best metal CO_2 electroreduction catalysts. In addition, the cubanes exhibit a scaling relation that deviates from the transition metals [6] for all the studied charge states.

1.1 Adsorbate energies

Adsorbate free energies were calculated by treating all of the adsorbate's $3N$ degrees of freedom as vibrational and neglecting changes in the cubane vibrational modes due to the presence of adsorbates. [7, 8] The vibrational modes of each adsorbate were calculated within the harmonic oscillator approximation and used to determine the zero-point energies, entropies, and heat capacities necessary to convert the DFT electronic energies to free energies. [4, 7, 9] These contributions to the free energy ($G - E_{\text{elec}}$) are calculated with the RPBE functional from the optimized geometries and summarized in Table S1 at a temperature of 25°C.

Solvation effects at the solvent-cluster interface are accounted for approximately as described previously. [7, 8] These effects include a correction to the COOH* intermediate of 0.25 eV for hydroxyl that is indirectly bound to the surface through other atoms (R−OH*), [7, 10] and 0.1 eV for CO*. [7] No correction is applied to the OCHO* intermediates.

Table S2: Assumed fugacity for each non-adsorbed gas-phase species, along with zero-point energy correction, enthalpic temperature correction, entropy contribution, specified correction for the OCO backbone, and final chemical potential as calculated with RPBE.

Species	Fugacity (Pa)	ZPE (eV)	$\int C_P\, dT$ (eV)	$-TS$ (eV)	E^c_{OCO} (eV)	μ (eV)
CO	101325	0.13	0.09	−0.61	–	−0.39
CO_2	101325	0.31	0.10	−0.66	0.45	0.20
HCOOH	19	0.89	0.11	−0.99	0.45	0.46
H_2	101325	0.27	0.09	−0.40	–	−0.04
H_2O	3534	0.57	0.10	−0.67	–	0.00
H_2S	1013	0.40	0.10	−0.75	–	−0.25
COS	1013	0.24	0.10	−0.84	0.45	−0.05
COOHS	1013	0.63	0.14	−0.99	0.45	0.23
H_2CSO_2	1013	0.97	0.14	−0.99	0.45	0.57

1.2 Non-adsorbed species and gas-phase correction

The chemical potentials of gas-phase species were obtained by standard ideal gas methods by using the calculated electronic energy and vibrational modes. [4, 9] In Table S2 we summarize the components of the calculated free energies, including the zero-point energies, enthalpic temperature corrections and entropy contributions. The free energies were calculated at a temperature of 25°C and pressure contributions were taken at a standard of 1 atm for all species other than water and formic acid. The free energy of water was calculated at a fugacity of 3534 Pa (the vapor pressure of water), while the free energy of formic acid was calculated at a fugacity of 19 Pa to represent 1 M HCOOH. [11] The fugacities of H_2S and COS were referenced at 1013 Pa, but the conclusions drawn from Figure 5 of the main text are largely insensitive to this choice.

As the RPBE functional was used, we also included a systematic correction to the electronic energies of gas-phase species containing an OCO backbone as in Ref. 7 (E^c_{OCO} in Table S2). Because we considered the COS molecule in the analysis of the cluster stability, we performed a similar statistical sensitivity analysis as in Ref. 7 to see if the RPBE error was also present in species with an OCS or SCS backbone. For the sensitivity analysis we considered the set of S-containing reactions in Table S3, based on analogs to the set originally considered in Ref. 7 for species containing O. The analysis consists of applying a systematic correction to an individual chemical species and determining the mean absolute error (MAE) with respect to the experimental values for the reactions in Table S3. For a given chemical species, the optimal correction is obtained by minimizing the MAE of all reactions, including the "bystander reactions" that are not affected by the correction.

We summarize the error of the reactions without corrections in Table S4, where it can be seen that reactions containing OCS and CSC also suffer from systematic errors as with the OCO species. [7] For the sensitivity analysis, we considered adding a single systematic correction to the species containing an XCX backbone, where X can be O or S. As seen in Figure S1, the optimal correction was found to be +0.44 eV, nearly identical to the RPBE error in the OCO backbone. [7] We also summarize the improvements in Table S4, finding the inclusion of such a correction to the OCS and SCS species can reduce the total MAE of the reaction set from 0.27 eV to 0.06 eV. Thus the observed error in the OCO backbone as described by RPBE is more general and can be extended to gas-phase species also containing S. For simplicity we use

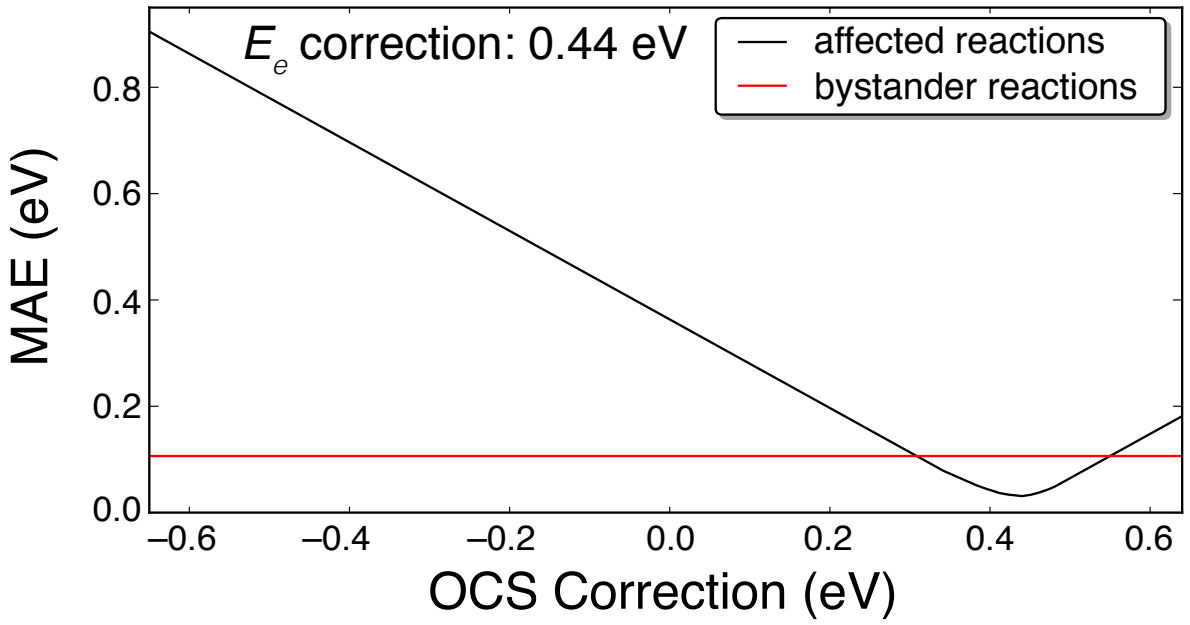

Figure S1: The sensitivity analysis to the enthalpy correction for the gas-phase species containing an OCS or CSC backbone. The reactions in Table S3 that include CS_2 or OCS are denoted as "affected reactions", while those that do not contain these species are labeled "bystander reactions". The mean absolute error is the absolute error per reaction as compared to NIST values.

the +0.45 eV correction originally found necessary for OCO, which is found to lead to a nearly identical improvement as summarized in Table S4. We note that without any correction to COS, the qualitative conclusions on the cubane stability in the presence of CO would not change for the -2 charge state.

1.3 Influence of the cluster charge and spin

As indicated in the text, both the charge state and magnetic and electronic spin configurations affect the calculated total energies, and therefore the reported binding energies. For each charge state and adsorbate, we independently varied both the magnetic and electronic spin contributions of the cluster to determine the lowest energy structure. This involved testing the 16 permutations of the magnetic moments in each cluster and calculating the energies for a range of corresponding electronic spin states. All reported binding energies are from the lowest energy configuration for each adsorbate and charge state. We note that the RPBE functional, like other forms of semilocal exchange-correlation functionals, are fundamentally unable to fully describe the total spin in these types of systems. Therefore the calculated spin states are used only as a guide to determine the lowest energy structures and to extract trends.

To investigate the role of the cluster charge state, we considered charges ranging from $q = 0$ to -2 for each cluster composition. We note that the charge state of the clusters are strongly dependent on the chemical environment and do not attempt to justify which charge states may be the most prevalent for a given cluster composition. These details will ultimately be determined by a variety of external factors such as the supporting structure and the type of solvent or electrolyte. We find that the Fermi levels of all isolated Ni-containing clusters fall below

Table S3: Reactions analyzed for the gas-phase ΔH comparisons (at 25° and 101325 Pa) based on those in Ref. 7.

Rxn	Stoichiometry
0	$CS_2 + H_2 \longrightarrow CS + H_2S$
1	$CS_2 + 4\ H_2 \longrightarrow CH_4 + 2\ H_2S$
2	$3\ H_2 + CS \longrightarrow CH_4 + H_2S$
5	$CS_2 + 3\ H_2 \longrightarrow CH_3SH + H_2S$
6	$2\ H_2 + CS \longrightarrow CH_3SH$
7	$CS_2 + 3\ H_2 \longrightarrow 1/2\ CH_3CH_2SH + 3/2\ H_2S$
8	$2\ H_2 + CS \longrightarrow 1/2\ CH_3CH_2SH + 1/2\ H_2S$
9	$CS_2 + 10/3\ H_2 \longrightarrow 1/3\ C_3H_8 + 2\ H_2S$
10	$7/3\ H_2 + CS \longrightarrow 1/3\ C_3H_8 + H_2S$
11	$CS_2 + 7/2\ H_2 \longrightarrow 1/2\ C_2H_6 + 2\ H_2S$
12	$5/2\ H_2 + CS \longrightarrow 1/2\ C_2H_6 + H_2S$
13	$CS_2 + 3\ H_2 \longrightarrow 1/2\ C_2H_4 + 2\ H_2S$
14	$2\ H_2 + CS \longrightarrow 1/2\ C_2H_4 + H_2S$
15	$CS_2 + 11/4\ H_2 \longrightarrow 1/4\ CH_2{=}CHCH{=}CH_2 + 2\ H_2S$
16	$7/4\ H_2 + CS \longrightarrow 1/4\ CH_2{=}CHCH{=}CH_2 + H_2S$
21	$H_2S + CO \longrightarrow COS + H_2$
22	$H_2O + CS \longrightarrow COS + H_2$
23	$CO_2 + H_2S \longrightarrow COS + H_2O$
24	$CS_2 + H_2O \longrightarrow COS + H_2S$

Table S4: Reaction enthalpies (in eV) of the reactions listed in Table S3 as calculated with the RPBE functional, shown without any corrections (ΔH_{unc}) and corrected with +0.45 eV (ΔH_{cor}) for species containing an OCS or SCS backbone. All errors are reported to the reference values from NIST (ΔH_{ref}). [12]

Rxn	ΔH_{ref}	ΔH_{unc}	error	ΔH_{cor}	error
0	1.48	1.82	0.34	1.37	−0.11
1	−2.41	−1.97	0.44	−2.42	−0.01
2	−3.90	−3.79	0.10	−3.79	0.10
5	−1.66	−1.22	0.44	−1.67	−0.01
6	−3.14	−3.04	0.10	−3.04	0.10
7	−1.77	−1.29	0.48	−1.74	0.03
8	−3.25	−3.11	0.14	−3.11	0.14
9	−2.00	−1.53	0.47	−1.98	0.02
10	−3.48	−3.35	0.13	−3.35	0.13
11	−2.07	−1.62	0.46	−2.07	0.01
12	−3.56	−3.44	0.12	−3.44	0.12
13	−1.37	−0.95	0.41	−1.40	−0.04
14	−2.85	−2.78	0.07	−2.78	0.07
15	−1.36	−0.94	0.42	−1.39	−0.03
16	−2.84	−2.76	0.08	−2.76	0.08
21	−0.07	−0.52	−0.44	−0.07	0.01
22	−1.83	−2.22	−0.38	−1.77	0.07
23	0.35	0.33	−0.02	0.33	−0.02
24	−0.35	−0.40	−0.04	−0.40	−0.04

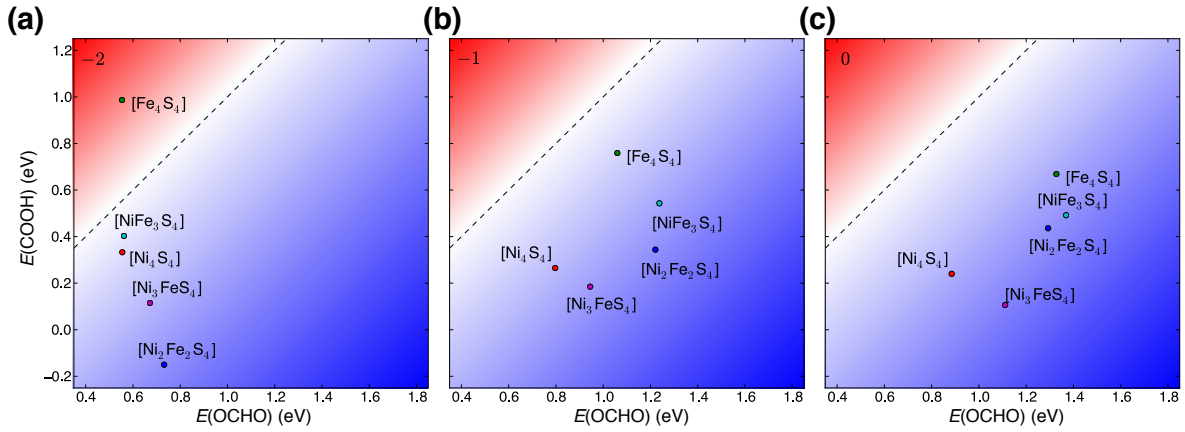

Figure S2: The calculated binding energies of the COOH* and OCHO* intermediates for the studied cubane compositions in the -2 (a), -1 (b), and 0 (c) charge states. The dashed lines in each plot delineate equal binding energies for the two intermediates and the cross-over between the pathways to produce HCOOH (top-left) and CO (bottom-right). All cubanes containing a Ni favor the COOH* intermediates, and thus favor the formation of CO relative to HCOOH for all charge states. The $[Fe_4S_4]$ cubane only favors the OCHO* intermediate for the -2 charge state, and behaves like the Ni-contaning cubanes for the other charge states.

that calculated for the isolated $[Fe_4S_4]$ cubane. When considering that the experimentally synthesized $[Fe_4S_4]$ cubane structures are found to have a charge of -2, [5] these results do not exclude the possibility of such charge states for the Ni-containing clusters.

In Figure S2, we show that all of the studied cubanes favor the COOH* intermediate for the 0 and -1 charge states, while further reduction leads to qualitative changes in the selectivity. Our calculations suggest that the $[Fe_4S_4]^{-2}$ cubane, similar to that synthesized experimentally, [5] would be the only cluster composition more selective toward the formation of OCHO* and HCOOH (Figure S2).

In Figure S3, we show the role of the cluster charge state in the context of the activity model of Ref. 6. The trendlines of the different cubane compositions, shown by the dotted lines in Figure S3, all deviate from the dark line representing the transition metal CO_2 electroreduction catalysts. [6] As the cluster charge goes from 0 to -2, the cubane trendline deviates significantly more from the transition metals and falls over a much more active region of the activity volcano. Additionally, the results suggest that these types of Ni-containing cubanes will become more active as they are reduced, in contrast to the pure Fe_4S_4 cluster (Figure S3). Thus independent of the cluster charge state, the Ni-containing cubanes are predicted to be comparable to or more active than the best metal CO_2 electroreduction catalysts.

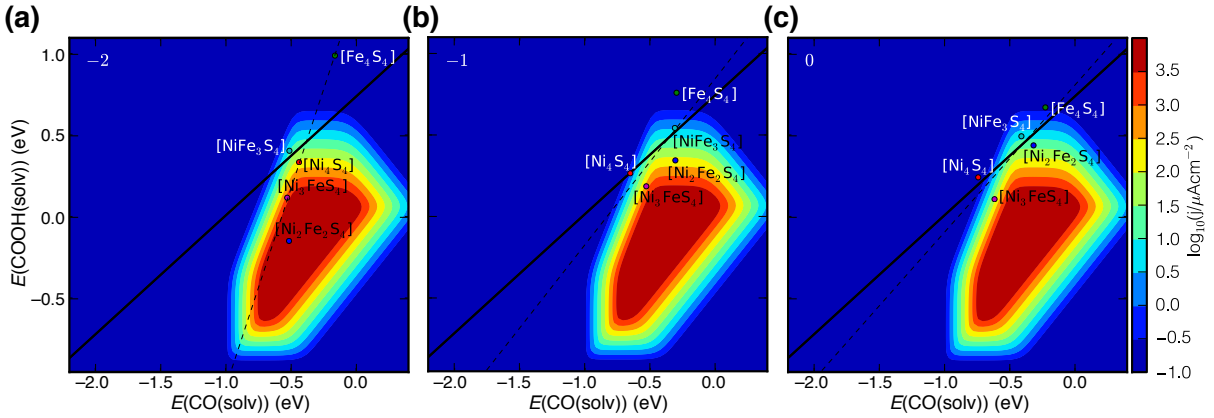

Figure S3: Kinetic volcano for CO evolution current at 0.3 V overpotential from Ref. 6, shown with the studied cubane compositions in the -2 (a), -1 (b), and 0 (c) charge states. The solid line represents the trend line for the (211) step of transition metals, which does not pass over the top of the volcano. The dashed line represents the linear best fit of the $[Ni_xFe_{4-x}S_4]^q$ ($x = 0, \ldots, 4$), which deviates from the transition metals for all charge states. While the noble metals reside near the optimum of the trend line, [6] the cubanes containing at least one Ni are predicted to be comparably or much more active in the electroreduction of CO_2 to CO.

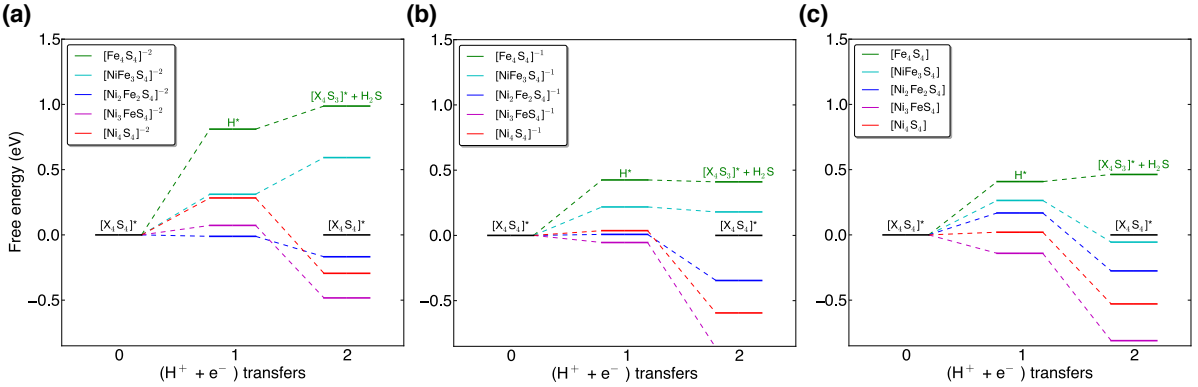

Figure S4: The calculated free energy pathway for dissociation of H_2S from the studied cubane compositions in the -2 (a), -1 (b), and 0 (c) charge states. The pathway follows that for the hydrogen evolution reaction (HER) for the first proton-electron transfer step, but splits into to two distinct pathways for the second proton-electron transfer step. The black line shows the energy of producing H_2 and returning to the normal cluster composition ($[X_4S_4]$), while the other lines show the free energies of stripping a S atom from the cluster as H_2S, leaving a cluster of composition $[X_4S_3]$. Clusters with more than 1 Ni are found to favorably desorb H_2S under HER conditions.

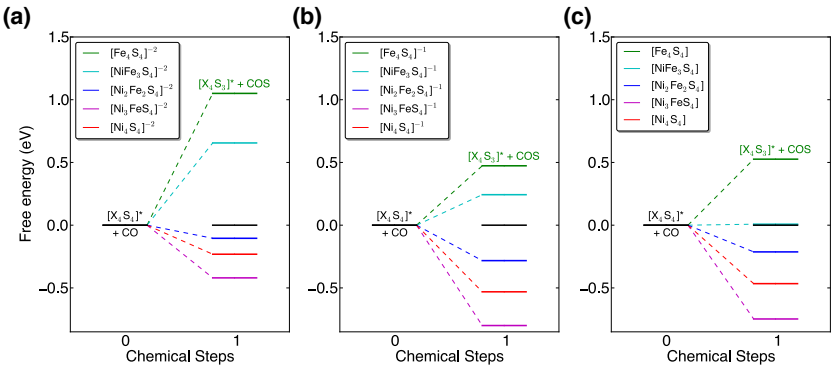

Figure S5: The calculated free energy pathway for dissociation of COS from the studied cubane compositions in the -2 (a), -1 (b), and 0 (c) charge states. The normal cluster composition ($[X_4S_4]$) with CO is used as a reference energy compared to the free energies of stripping a S atom from the cluster as COS, leaving a cluster of composition $[X_4S_3]$. Clusters with more than 1 Ni are found to generally favor the desorption of COS, while the $[Ni_2Fe_2S_4]^{-2}$ is only marginally stable to COS dissociation at the specified conditions.

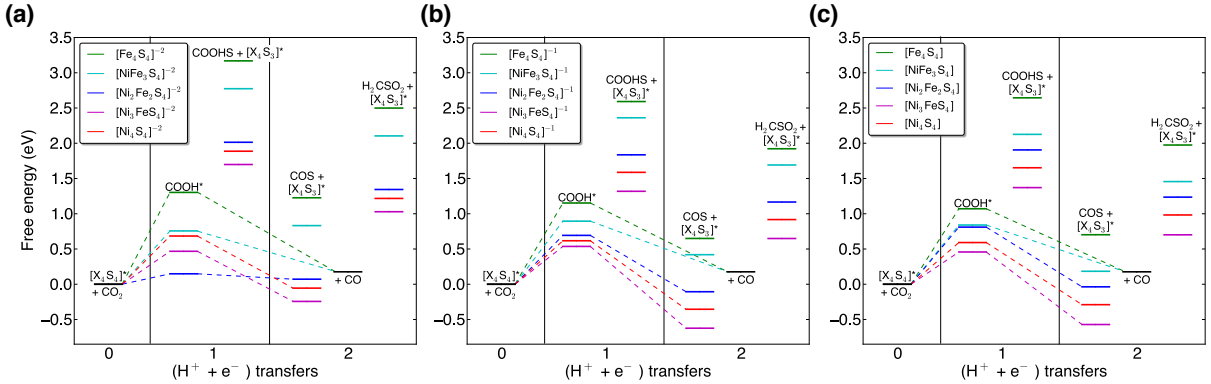

Figure S6: The calculated free energy pathway for different dissociation mechanisms from the COOH* intermediate for the studied cubane compositions in the -2 (a), -1 (b), and 0 (c) charge states. The normal cluster composition ($[X_4S_4]$) with no adsorbates is used as a reference energy compared to the free energies of stripping a S atom from the cluster under subsequent proton-electron transfers to CO_2, leaving a cluster of composition $[X_4S_3]$ and a dissociated COOHS or H_2CSO_2. For all charge states and compositions, cubane dissociation in the presence of the COOH* intermediate as COOHS or H_2CSO_2 is less favorable than producing CO or COS (see Fig. S5).

References

[1] Mortensen, J. J.; Hansen, L. B.; Jacobsen, K. W. Real-space grid implementation of the projector augmented wave method. *Phys. Rev. B* **71**, 035109 (2005).

[2] Enkovaara, J. *et al.* Electronic structure calculations with GPAW: a real-space implementation of the projector augmented-wave method. *J. Phys. Condens. Matter* **22**, 253202 (2010).

[3] Hammer, B.; Hansen, L. B.; Nørskov, J. K. Improved adsorption energetics within density-functional theory using revised Perdew-Burke-Ernzerhof functionals. *Phys. Rev. B* **59**, 7413–7421 (1999).

[4] Bahn, S. R.; Jacobsen, K. W. An object-oriented scripting interface to a legacy electronic structure code. *Comput. Sci. Eng.* **4**, 56–66 (2002).

[5] Wong, G. B.; Bobrik, M. A.; Holm, R. H. Inorganic derivatives of iron-sulfide-thiolate dimers and tetramers: Synthesis and properties of the halide series $[Fe_2S_2X_4]^{2-}$ and $[Fe_4S_4X_4]^{2-}$ (X = Cl^-, Br^-, I^-). *Inorg. Chem.* **17**, 578–584 (1978).

[6] Hansen, H. A.; Varley, J. B.; Peterson, A. A.; Nørskov, J. K. Understanding trends in the electrocatalytic activity of metals and enzymes for CO_2 reduction to CO. *The Journal of Physical Chemistry Letters* **4**, 388–392 (2013).

[7] Peterson, A. A.; Abild-Pedersen, F.; Studt, F.; Rossmeisl, J.; Nørskov, J. K. How copper catalyzes the electroreduction of carbon dioxide into hydrocarbon fuels. *Energy Environ. Sci.* **3**, 1311–1315 (2010).

[8] Varley, J. B.; Nørskov, J. K. First-principles calculations of Fischer-Tropsch processes catalyzed by nitrogenase enzymes. *ChemCatChem* **5**, 732–736 (2013).

[9] Cramer, C. J. *Essentials of Computational Chemistry* (Wiley, 2004), 2 Edn.

[10] Tripković, V.; Skúlason, E.; Siahrostami, S.; Nørskov, J. K.; Rossmeisl, J. The oxygen reduction reaction mechanism on Pt(111) from density functional theory calculations. *Electrochem. Acta* **55**, 7975 – 7981 (2010).

[11] Durand, W. J.; Peterson, A. A.; Studt, F.; Abild-Pedersen, F.; Nørskov, J. K. Structure effects on the energetics of the electrochemical reduction of CO_2 by copper surfaces. *Surf. Sci.* **605**, 1354 – 1359 (2011).

[12] Afeefy, H.; Liebman, J.; Stein, S. *Neutral Thermochemical data in NIST Chemistry WebBook, NIST Standard Reference Database Number 69* (National Institute of Standards and Technology, Gaithersburg MD, USA, 2010).